JOURNAL OF GEOPHYSICAL RESEARCH, VOL. 113, D15126, doi:10.1029/2008JD009889, 2008

Click Here for Full Article

Cloud patterns lee of Hawaii Island: A synthesis of satellite observations and numerical simulation

Yang Yang,[1,2] Shang-Ping Xie,[2] and Jan Hafner[2]

Received 30 January 2008; revised 13 April 2008; accepted 29 April 2008; published 15 August 2008.

[1] Standing well above the trade wind inversion, Hawaii Island (maximum elevation ~4.2 km) splits the northeast trade winds and induces a westerly reverse flow in the wake. Satellite observations and regional model simulations are used to investigate circulation effects on lee cloud formation during summer. Over the island, the cloud distribution is consistent with orographic-induced vertical motions. Over the lee ocean, our analysis reveals a cloud band that extends southwestward over a few tens of kilometers from the southwest coast of the island. This southwest lee cloud band is most pronounced in the afternoon, anchored by strong convergence and maintained by in situ cloud production in the upward motion. Such an offshore cloud band is not found off the northwest coast, an asymmetry possibly due to the Coriolis effect on the orographic flow. Off the Kona coast, the dynamically induced westerly reverse flow keeps the wake cool and nearly free of clouds during the day. Along the Kona coast, clouds are blown offshore from the island by the easterly trades in the afternoon in a layer above the reverse flow. Deprived of in situ production, these afternoon Kona coast clouds dissipate rapidly offshore. At night, the offshore land/valley breezes converge onto the onshore reverse flow, and a cloud deck forms on and off the Kona coast, bringing nighttime rain as observed at land stations. To illustrate the circulation effect, lee cloud formation is compared between tall Hawaii and short Kauai/Oahu Islands, which feature the flow-around and flow-over regimes, respectively. Effects of trade wind strength on the leeside cloudiness are also studied.

Citation: Yang, Y., S.-P. Xie, and J. Hafner (2008), Cloud patterns lee of Hawaii Island: A synthesis of satellite observations and numerical simulation, *J. Geophys. Res.*, *113*, D15126, doi:10.1029/2008JD009889.

1. Introduction

[2] The island of Hawaii is the largest of the Hawaiian island chain, with a diameter of roughly 140 km. Its topography is dominated by two volcanic mountains, Mauna Loa and Mauna Kea (Figure 1a), both exceeding 4100 m in elevation. Climatologically, the northeast trade winds of 4–10 m s^{-1} are persistent (70%) throughout the year, especially in summer (90%) [*Schroeder*, 1993]. For a stratified airflow past a circular mountain, the Froude number (Fr = *U*/Nh, where *U* is the upstream wind speed, N the Brunt-Väisälä frequency, and h is the mountain height) is an important control parameter for flow regimes [*Smith*, 1989]. In a numerical model without surface friction and diabatic heating, *Smolarkiewicz and Rotunno* [1989] obtain a pair of vertically oriented vortices lee of a circular mountain for Fr 0.1–0.5. For Hawaii Island, under the summer trade wind flow with N = 0.01 s^{-1} and *U* = 8 m s^{-1}, Fr is 0.2 [*Carbone et al.*, 1998], putting its wake in the regime of lee vortex occurrence. Both U and N display significant variations in the vertical and time, introducing some ambiguity in estimating Fr and its prediction of flow regime [*Reinecke and Durran*, 2008].

[3] The wake of Hawaii Island has been detected from ship [*Patzert*, 1969] and aircraft [*Nickerson and Dias*, 1981; *Smith and Grubišić*, 1993] observations and simulated by high-resolution models [*Yang et al.*, 2005; *Shen et al.*, 2006]. The Hawaii wake consists of two quasi-steady eddies with strong reverse flow along the wake axis [*Smith and Grubišić*, 1993]. Strong wind curls in the wake force ocean circulation changes, triggering active ocean-atmosphere interaction that sustains the island effect over a long distance [*Xie et al.*, 2001; *Hafner and Xie*, 2003; *Yu et al.*, 2003; *Sakamoto et al.*, 2004; *Sasaki and Nonaka*, 2006]. In addition to the dynamical forcing, the land surface thermal forcing of the island significantly affects the island-scale circulations as seen in the diurnal cycle [*Leopold*, 1949; *Chen and Nash*, 1994; *Yang and Chen*, 2003]. The thermal forcing is particularly important over the large and tall island of Hawaii [*Yang and Chen*, 2008].

[4] The far-field effect of the Hawaiian islands on surface wind has been mapped from satellite microwave scatterometers [*Xie et al.*, 2001; *Chelton et al.*, 2004]. Land emission renders microwave instruments ineffective within 50 km of islands. Furthermore, microwave instruments do not have high enough resolution to observe fine structures of island effects in the near field. Over the sea in situ observations are

[1]National Institute of Water and Atmosphere Research, Wellington, New Zealand.
[2]International Pacific Research Center, SOEST, University of Hawaii at Manoa, Honolulu, Hawaii, USA.

Copyright 2008 by the American Geophysical Union.
0148-0227/08/2008JD009889$09.00

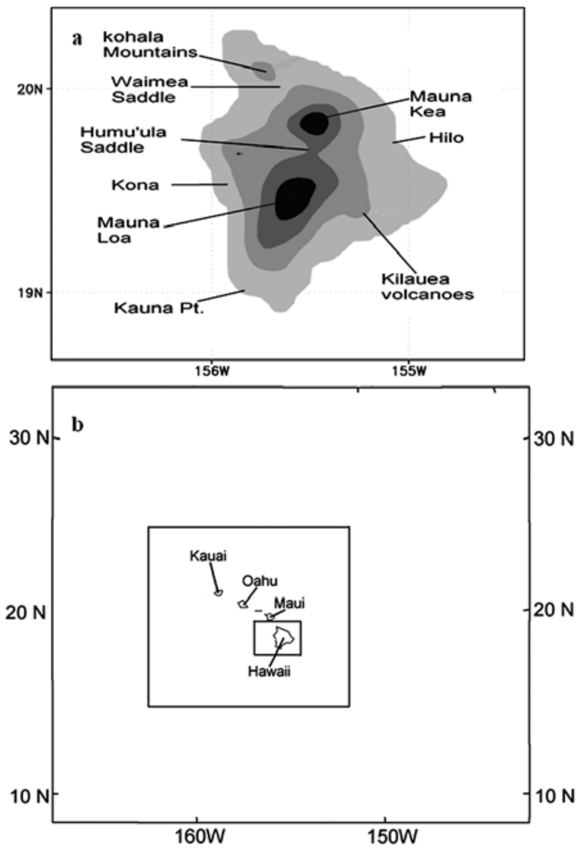

Figure 1. (a) Map of Hawaii Island, with terrain height in gray shading at 1000-m intervals. (b) Three model domains with resolution of 27, 9, 3 km, respectively.

few and inadequate for high-resolution mapping. The present paper attempts to study island effects on the lee circulations from satellite visible and infrared observations of clouds, which cover both land and sea at high resolution. The cloud distribution and its diurnal variations over and around an island reflect the effects of its dynamical and thermal forcing.

[5] Using a similar method, *Yang et al.* [2008a] detect a pronounced diurnal cycle in cloud occurrence trailing islands of Kauai/Niihau and Oahu for as much as 100 km during summer. These lee cloud bands develop before noon, peak in cloudiness in early afternoon, and decay in late afternoon. Results from numerical simulations indicate a thermal wake mechanism for this diurnal cycle of the trail clouds: during the day, the warm advection by the trades from the warm island lowers the atmospheric pressure and drives a surface convergence in favor of cloud formation in the wake. Conversely, the cold advection during night suppresses cloud formation. There are reasons to expect, however, that similar trail clouds do not form the wake of Hawaii Island, where the reverse flow does not allow thermal advection from the island.

[6] There is evidence that the reversed flow affects precipitation on the Kona coast of Hawaii Island. There, *Yang and Chen* [2003] reported an evening rainfall maximum from surface observations and greater rainfall under strong than weak trade wind conditions. They speculated that the nighttime rainfall maximum is caused by the convergence between the dynamically induced westerly return flow in the wake and the land breezes. Numerical simulations [*Yang et al.*, 2008b] support this hypothesis but lack of observations over the waters lee of Hawaii prevent it from being further tested.

[7] From satellite observations, this study maps a summer cloud climatology over Hawaii Island and its wake (including the diurnal cycle) and then identifies major cloud features in the wake. Aided with numerical simulations, we investigate mechanisms for lee cloud formation near the island. Our analysis reveals several new cloud features. In particular, we show that a long cloud line develops in the early afternoon in the southwestern lee and is associated with a strong surface convergence line.

[8] The rest of this paper is organized as follows. Section 2 describes the data and model simulation. Section 3 presents summer mean cloud maps from satellite, and section 4 investigates cloud formation using simulation results. Section 5 examines the sensitivity of the cloudiness to the trade wind strength. Section 6 is a summary.

2. Data and Model

[9] Polar orbit satellites Terra and Aqua fly over Hawaii around 11:00 and 14:00 Hawaiian standard time (HST) during the daytime, respectively. In this study, cloud mask data from the Moderate Resolution Imaging Spectroradiometer (MODIS) on Terra at 11:00 HST and Aqua at 14:00 HST during June–August of 2004 and 2005 are used to calculate frequency of cloud occurrence over the Hawaii region, defined as the number of days with cloud cover divided by the total number of days considered. For both Terra and Aqua, only the daytime cloud mask data are used because of known problems of more clouds than actual over the ocean and false cloud detection over land using infrared data alone during the nighttime (http://modis-atmos.gsfc.nasa.gov/MOD35_L2/qa.html). For the daytime cloud mask data, the only known problem is the cloud detection near the coastline. MODIS has a 2330 km wide swath and a repeat cycle of 16 days, during which one or two swaths do not cover the entire Hawaiian island chain. In this study, we use the swaths covering the entire state.

[10] To capture the diurnal cycle better, we use the data from the geostationary satellite GOES-10 visible channel-1 (1-km resolution nadir) and infrared (IR) channel-5 (4-km resolution nadir) with 15-minute intervals in August 2005. Climatologically, the occurrence of the northeast trade winds is 92% in August, the highest month of the year. Thus August is representative of the entire summer. The radiance from visible channel-1 is converted to effective albedo, which is smaller over the sea under clear sky than in cloudy conditions. The radiance from the IR channel-5 is converted to brightness temperature. The effective albedo is correlated with the cloud amount, but this relationship is affected by the diurnal variations in solar altitude.

[11] We use the fifth-generation Mesoscale Model (MM5, version 3) developed at Pennsylvania State University and National Center for Atmospheric Research (NCAR) [*Dudhia*, 1993]. It is a nonhydrostatic primitive-equation model with the terrain-following sigma vertical coordinate. In this study, there are 34 sigma levels in total (The sigma

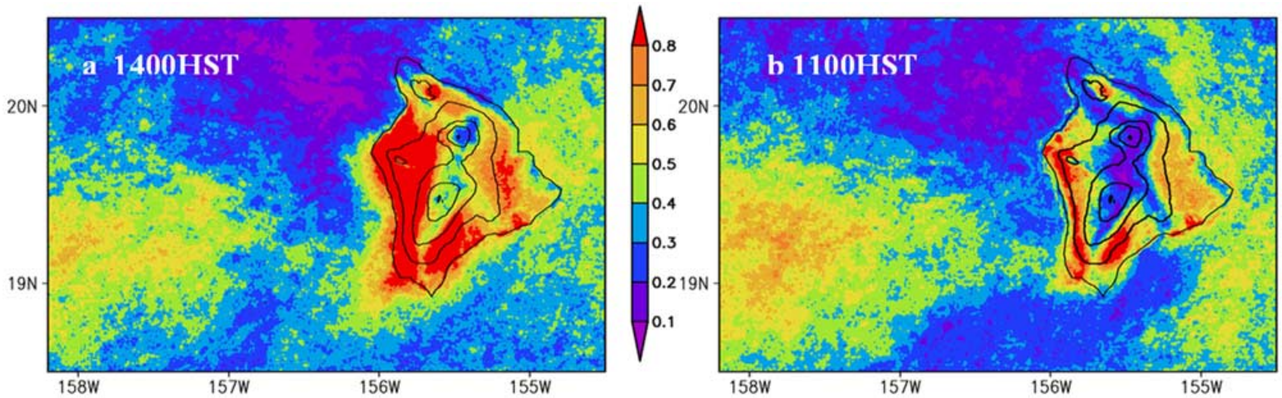

Figure 2. Cloud frequency for Hawaii Island during the summers of 2004 and 2005 at (a) 14:00 HST from MODIS Aqua and (b) 11:00 HST from MODIS Terra. Land topography is shown in solid contours with 1000-m interval.

levels are: 1, 0.999, 0.997, 0.994, 0.991, 0.988, 0.985, 0.980, 0.97, 0.945, 0.91, 0.865, 0.82, 0.79, 0.76, 0.73, 0.7, 0.67, 0.64, 0.61, 0.58, 0.55, 0.52, 0.475, 0.425, 0.375, 0.325, 0.275, 0.225, 0.175, 0.125, 0.075, 0.025, 0.) from the surface to 100 hPa, with 13 of them (0, 8, 24, 47, 71, 95, 119, 159, 239, 442, 734, 1121, 1455 m) below 1500 m to resolve the boundary layer. Three two-way nesting domains are used with horizontal resolutions of 27, 9, and 3 km (Figure 1b). The Grell cumulus parameterization (employed only for 27- and 9-km resolution domains only), a grid-scale warm rain process [*Hsie et al.*, 1984], a cloud radiation scheme [*Dudhia and Moncrieff*, 1989], and *Hong and Pan*'s [1996] boundary layer scheme are used. An advanced land surface model (LSM) [*Chen and Dudhia*, 2001] is coupled with MM5, with four layers at depths of 10, 40, 100, and 200 cm. The vegetation type, soil type, and vegetation fraction were compiled from the U.S. Geological Survey (USGS) 1:100,000-scale land-use land-cover level II data for Hawaii [*USGS*, 1986]. The soil types were also compiled from the USGS data based on soil surveys in Hawaii [*Foote et al.*, 1972; *Sato et al.*, 1973], using the procedures described by *Zhang et al.* [2005] on a 30″ grid. Validating the model against observations during the Hawaiian Rainband Project (HaRP, 11 July–25 August 1990), *Yang et al.* [2005] show that with the improved land surface data of Zhang et al., the MM5/LSM simulates well the island-scale circulations and their diurnal cycle.

[12] Here we conduct simulations for June–August of 2005 with MM5/LSM, following the procedures of *Yang et al.* [2005] as described below. The MM5/LSM is spun up for two months ending 31 May 2005, to obtain appropriate initial soil moisture and soil temperature fields. From 1 June to 31 August, the model is initialized daily at 1200 UTC using the 24-hour (h) forecast of the previous day for soil moisture and soil temperature, and NOAA's Global Forecasting System (GFS) $1^\circ \times 1^\circ$ analysis for other fields. The GFS analysis is also used for the lateral boundary conditions for the outmost domain. The MM5/LSM is integrated forward for 36 h. The snapshots are saved every two hours from the 12th to the 36th hour for each daily simulation. A climatologically diurnal cycle is constructed by averaging 92 snapshots from 1 June to 31 August 2005. Year-to-year variability is small in summer and the 2005 summer is representative of the summer climatology.

3. Satellite Cloud Observations

[13] This section uses MODIS and GOES-10 data to investigate the daytime distribution and diurnal cycle of cloud occurrence over and lee of the island of Hawaii.

3.1. Daytime

[14] Over the island (Figure 2), clouds are infrequent over Mts. Kea and Loa, which stand above the inversion and split the incoming trade winds. High cloud occurrence is found on the slopes during the day. Over the middle and upper slopes, cloud frequency increases from morning to afternoon. Narrow bands of infrequent cloud occurrence are found lee of major mountain ridges including Kohala Mountains in the northwest Hawaii, the Kilauea Volcanoes in the southeast, and Mt. Loa's south ridge in the south, caused by the descent of trade wind flow.

[15] In the morning, it is nearly free of cloud over the waters off the Kona coast but clouds develop there in the afternoon (Figure 2). Cloud frequency amounts to 0.2–0.4 at 14:00 HST offshore. Hereafter we call it the Kona coastal (KC) cloud band, which extends 20 km offshore in the afternoon. In the southwestern lee, clouds begin to appear in the morning and develop in afternoon into a well-defined cloud band that tilts in the southwest direction and extends for 70 km. We call it the southwest (SW) lee cloud band. The KC and SW lee cloud bands are identified as regions of high albedo in the afternoon from the radiance of GOES-10 visible channel (Figures 3a and 3b). To our knowledge, neither the KC nor the SW lee cloud band has been described and studied in the literature, and they are the focus of this paper. Our model results show that they are caused by mutually distinct mechanisms (section 4).

[16] Figures 4a and 4b show distance-time sections of GOES albedo, tracking the evolution at 15-minute intervals of the SW lee and KC cloud bands, respectively. Over the southwestern lee, cloud production occurs mainly in the afternoon, especially over land. The downstream propagation of clouds from the island is pronounced at a speed of 3 m s^{-1}, much smaller than the typical wind speed at the

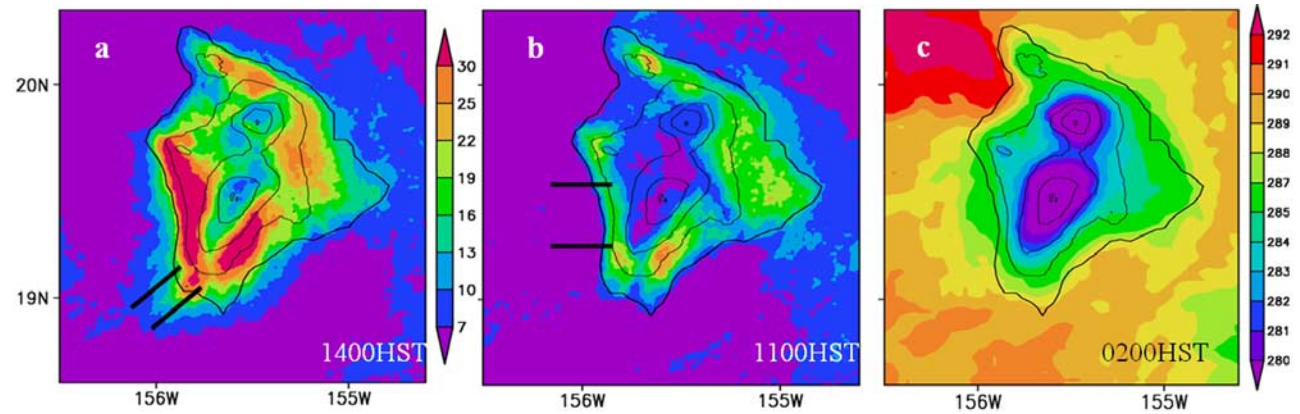

Figure 3. Mean effective albedo (%) at (a) 14:00 and (b) 11:00 HST during August 2005 from GOES-10 visible channel. (c) IR temperature at 02:00 HST during August 2005 from GOES-10 IR channel-5.

cloud level (8–10 m s^{-1}). Model simulations show that local cloud production by upward motion is substantial in the formation of the SW lee cloud band (section 4). Off the Kona coast, the westward propagation of clouds is notable (Figure 4b) at a speed of 1–1.5 m s^{-1} comparable to the wind speed at that level, but it has a limited range. Model results suggest that the KC cloud band is due to the offshore advection of land convective clouds around the base of the trade wind inversion. This is in sharp contrast with smaller and shorter islands of Kauai and Oahu, lee of which a cloud band develops in the early afternoon from the coast with a great downstream extension (~100 km) [*Yang et al.*, 2008a]. This difference in lee cloud pattern between Hawaii and Kauai/Oahu islands is due to that in wake circulation as discussed in section 4.

3.2. Nighttime

[17] Figure 3c shows the nighttime infrared brightness temperature from GOES. Since sea surface temperature variations over the Hawaii waters are small (<1 K), IR brightness temperature variations over the sea is due mainly to the effects of cloud/water vapor. IR temperature is high in the southwestern lee, indicating that the afternoon cloud band there has dissipated by 02:00 HST. A pronounced IR temperature maximum is found off the northwestern coast of the island as the strong descent of the trade wind flow brings dry air from higher levels, consistent with HaRP aircraft data [*Smith and Grubišić*, 1993; *Yang and Chen*, 2003].

[18] At night, IR temperature is low (284–287 K) in the wake, especially over the waters just off the Kona coast, indicating strong cloud production there. This is consistent with in situ rainfall observations showing a nighttime rainfall maximum on the Kona coast. Figure 5 shows the diurnal rainfall frequency at Captain Cook on the central Kona coast during HaRP. The evening rainfall frequency maximum around 21:00 HST is associated with the development of land breezes [*Yang and Chen*, 2003]. Our IR observations suggest that that these nighttime raining clouds extend offshore.

4. Numerical Simulations

[19] This section uses model results to investigate the mechanisms for the KC and SW lee cloud bands. Figure 6

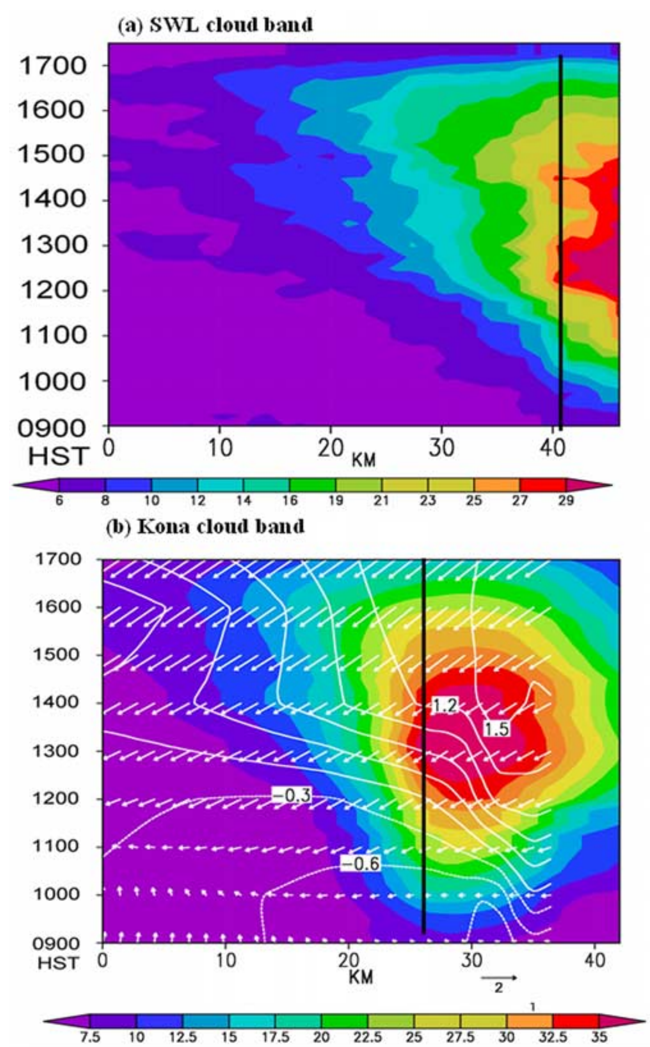

Figure 4. Time-Distance section of mean effective albedo (color shading) from GOES-10 visible channel-1 during August 2005 in (a) the southwest lee (between thick lines in Figure 3a) and (b) off the Kona coast (between thick lines in Figure 3b). Superimposed in Figure 4b are simulated horizontal wind velocity (vectors) and mixing ratio (g kg^{-1}) deviations from the daily mean (white contours) at 750 hPa. Thick solid lines show roughly the positions of coasts.

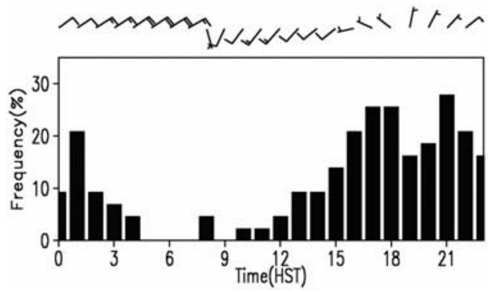

Figure 5. The diurnal rainfall frequency and daily mean wind velocity during the HaRP (11 July–24 August 1990) at a central Kona coast station (Captain Cook, 402 m elevation). Pennants, full barbs, and half barbs represent 5, 1, and 0.5 m s^{-1}, respectively. There is a rainfall frequency maximum in the evening when land breezes (easterly) begin to develop.

shows the daily mean horizontal and vertical velocities at 500 and 750 m, respectively. Tall Hawaii Island forces strong (12–14 ms^{-1}) southeasterly (northeasterly) winds along the northeastern (southeastern) coast, and easterly winds around the southern and northern tips. In the wake off the Kona coast, the dynamical forcing of the island produces a westerly reverse flow with speed up to 3 ms^{-1}. Temperature maxima are simulated in the northwestern and southwestern leeward areas, and lee of Kilauea Volcanoes in the southeastern island, as a result of adiabatic warming of strong descents of the trade wind flow aloft across mountain ridges [*Yang and Chen*, 2003].

[20] The aforementioned orographic downdrafts are in pair with orographic updrafts on the windward sides of the mountain ridges (Figure 6b). Strong rising motions up to 10 cm s^{-1} are also found off the lee coast of Kohala Mountains in the north, and in the southwestern lee near Kauna Point, associated with hydraulic jumps of the trade wind flow [*Smith and Grubišić*, 1993; *Yang et al.*, 2005]. The rising motion near Kauna Point shows a tendency to extend southwestward offshore.

4.1. Diurnal Variations

[21] Daily mean patterns may be viewed as resulted mainly from the dynamical forcing of island mountains while the diurnal deviations are due to island thermal forcing. The orographic effect over land is strong, and the vertical velocity pattern it induces remains similar during day and night (Figures 7b and 7e). As a result, vertically integrated cloud water (ICW) content is high throughout the day on the windward slope and the southeast slope of Mt. Loa (Figures 7c and 7f). At night, the windward cloud band is displaced in the offshore direction, consistent with HaRP [*Chen and Nash*, 1994] and satellite (Figure 3c) observations. During afternoon, elevated ICW is found over the windward, southeastern leeward Kona slopes as well as the leeward lowlands of Waimea Saddle in the northern island. Minimum ICW is simulated on high mountaintops of Mauna Loa and Kea. Thus the model captures the overall cloud pattern over the island.

[22] During the day sea breezes/anabatic flow develop on and off the Kona coast, enhancing the western reverse flow and the downward motion in the wake (Figures 7a and 7b), consistent with *Yang and Chen* [2008, their Figure 15a]. During night, land breeze/offshore flow develop, encountering the reverse flow in the wake and inducing upward motion in a broad region extending 20 km off the Kona coast. The offshore upward motion anchors a region of increased ICW, consistent with satellite (Figure 3c) and land-station (Figure 5) observations. Diurnal temperature variations in the wake are small (<0.25 K) as the westerly reverse flow prevents diurnal anomalies over land from penetrating. The reverse flow also keeps the wake cooler than both to the north and south.

[23] During afternoon, a sharp convergence line develops in the southwestern lee, emanating from Kauna Point and extending for at least 70 km offshore (Figure 7b). This convergence line anchors the SW lee cloud band observed from satellite (Figures 7c and 2a). During night, this SW lee convergence line weakens substantially (from 5–10 cm s^{-1} at 02:00 HST to nearly zero), and the associated cloud band dissipates (Figures 7e, 7f and 3c).

[24] To the north lee of Kohala Mountains, adiabatic orographic warming is enhanced by land surface heating during the day. The temperature maximum there is 2–3 K warmer in the afternoon than at night (Figures 7a and 7d). A

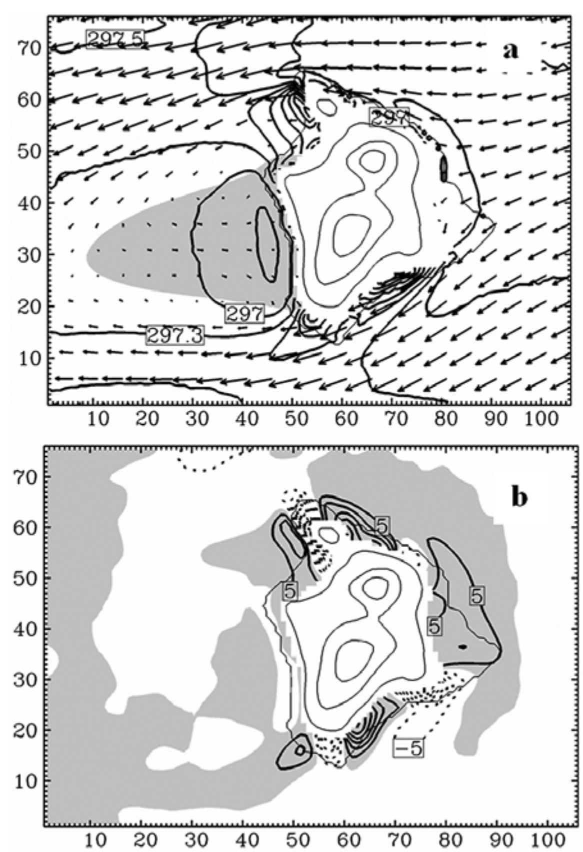

Figure 6. (a) Simulated daily mean winds (m s^{-1}) and potential temperature (K; 0.25-K interval) at 500 m above the sea level, with westerly reverse flow region being shaded. (b) Simulated daily mean vertical velocity at 750 m above the sea level (5 cm s^{-1} interval without zero contour), with uprising motion regions being shaded. Axis numbers denote grid points with 3-km resolution. The maximum wind vector is 13.5 m s^{-1}.

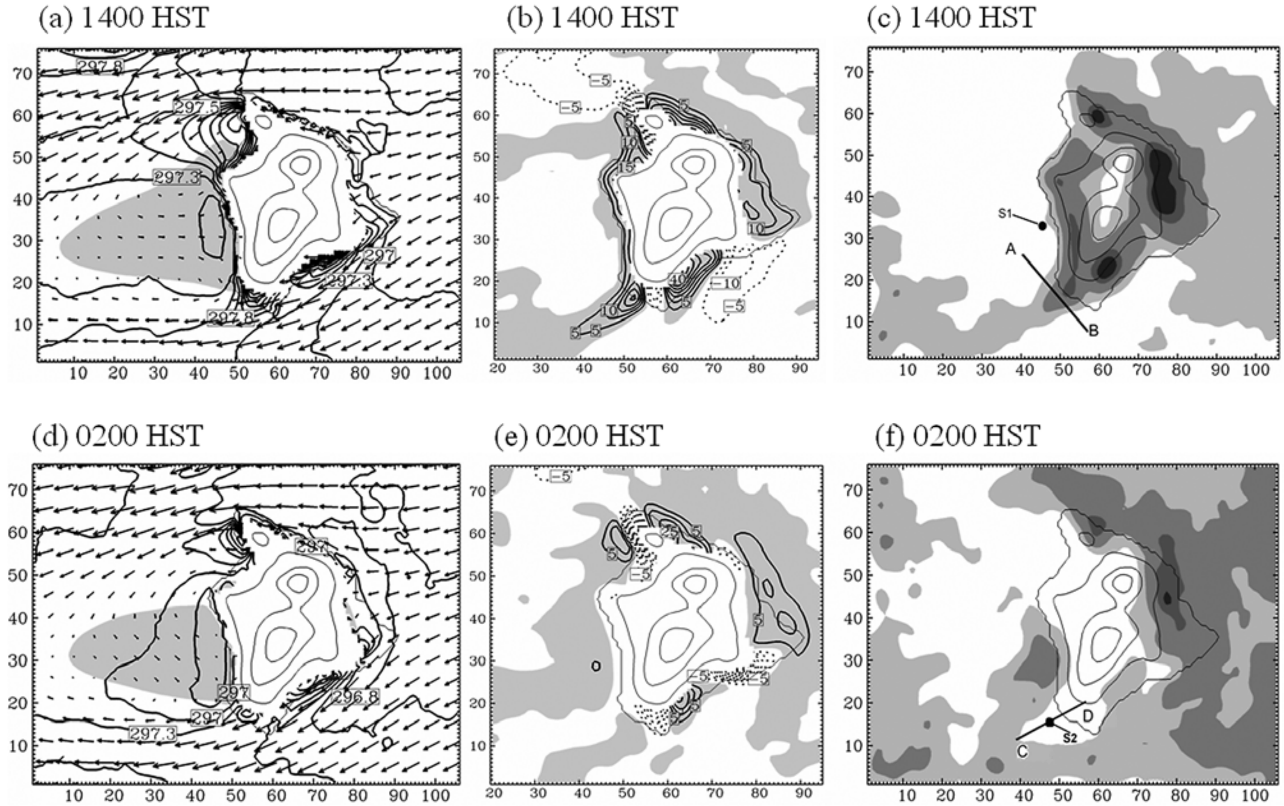

Figure 7. Simulated mean winds (m s^{-1}) and potential temperature (K; 0.25-K interval) at 500 m above the sea level at (a) 14:00 HST and (d) 02:00 HST, with the westerly reverse flow region being shaded. Simulated mean vertical velocity at 750 m above the sea level (5 cm s^{-1} interval without zero contour) at (b) 14:00 HST and (e) 02:00 HST, with uprising motion region being shaded. Simulated mean vertically integrated cloud water content (shading area with 0.04-mm interval) at (c) 14:00 HST and (f) 02:00 HST. Thick solid lines AB and CD in Figures 7c and 7f are transects for cross-section analysis. The maximum wind vector is 13.5 m s^{-1}. The black points denoted by S1 in Figure 7c and S2 in Figure 7f are geographic positions for the height-time cross-sections of Figure 10. Axis numbers denote grid points with 3-km resolution.

warm tongue extends far offshore during the afternoon (Figure 7a) possibly due to the advection of warm air over the island by the easterly winds there. As a result, This advective warming lee of Kohala may help extend weak upward motion westward (Figure 7b) by inducing surface wind convergence much the same as lee of Kauai and Oahu [*Yang et al.*, 2008a]. The afternoon convergence lee of Kohala is very weak compared to the SW lee convergence line emanating from Mauna Point. No cloud band forms over the ocean lee of Kohala during day or night in either the model (Figures 7c and 7f) or observations (Figure 3).

4.2. Southwest Lee Convergence Line

[25] The contrast between the northwestern (Konaha) and southern (Mauna Point) lees is quite striking in surface convergence and cloud formation during afternoon. We speculate that it might be due to the Coriolis force acting on orographic modulation of the northeast trades. Consider a simple situation with a uniform easterly flow impinging on a circular mountain. In the lee, the orographic effect accelerates the easterly flow north and south of the mountain while decelerating or even reversing the flow in the wake as in the case of Hawaii Island. The Coriolis force acting on such ageostrophic acceleration (deceleration) induces a northward (southward) wind component. The resultant meridional flow causes convergence (divergence) on the southern (northern) edge of the wake [e.g., *Hunt et al.*, 2001; *Olafsson and Bougeault*, 1997], as indeed happens in the model simulation and satellite cloud observations. In reality, this simple mechanism for causing north-south asymmetry is likely to be complicated by nonlinearity and interaction with the diurnal cycle. Nonlinearity of the orographic-induced flow probably helps sharpen the southern convergence into a narrow band in our model simulation.

[26] The rising motions in the southwest lee are much stronger in the afternoon than at night (Figures 7b and 7e). Figure 8 shows 2 pm–2 am HST difference in surface wind velocity. On the coast near Kauna Point, the rising motion is enhanced in the afternoon by the three-way convergence of the (anomalous) sea breezes/anabatic flow from the west and east slopes of the south extension of Mauna Loa, and from the southwest (perpendicular to the coast between Kauna and South Points). The convergence line extends offshore, separating the anomalous westerlies to the north and the anomalous south-to-southwesterly winds to the south. The formation mechanism for this sharp convergence line probably involves complicated interaction of thermal

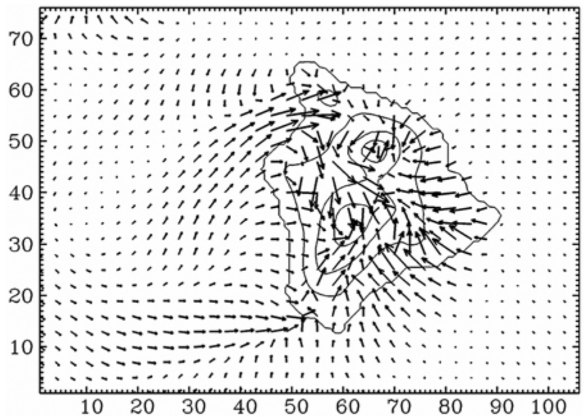

Figure 8. Wind difference at 50 m above the surface between 14:00 HST and 02:00 HST.

and dynamical forcing of the island, and requires further studies.

[27] Figure 9 captures the southwesterly sea breezes in an along-stream transect and the sea breezes converging the trades in a cross-stream section. Clouds form in the convergence line, with maximum cloud water at 2 km height riding above the upward motion. Figure 10b shows the time-pressure section of specific humidity deviations from the daily mean in the SW lee convergence line, along with horizontal wind velocity. Humidity displays a pronounced diurnal cycle below 750 hPa, with the maximum diurnal range of 2 g/kg at 875 hPa. Such a vertical structure of humidity diurnal cycle is consistent with the advection by variable vertical motion in the atmospheric boundary layer.

[28] The above results suggest that local cloud production by upward moisture transport is important for the afternoon SW lee cloud band. We have diagnosed the source/sink (production/dissipation) term of cloud water content (q_c) as the residual of total derivative, $S = \frac{\partial q_c}{\partial t} + u\frac{\partial q_c}{\partial x} + v\frac{\partial q_c}{\partial y} + w\frac{\partial q_c}{\partial z}$, where u, v and w are the three-dimensional wind components. The calculation is done between 11:00 and 14:00 HST and vertically integrated from the surface to 8 km. In the SW lee cloud band, the local production (source term) is greater than the advection by a factor of two (not shown).

[29] Figure 11 shows the full diurnal cycle across the SW lee cloud band, where rising motion develops during the day with a maximum of 15 cm s^{-1} at 14:00 HST. The maximum cloud water content occurs 2–3 hours later, consistent with GOES observations (Figure 4a). The maximum cloud water occurs when upward displacements, rather than vertical velocities, are at a maximum. Indeed, analysis of the equivalent potential temperature in this area shows that the maximum upward displacement of air parcel takes place around 16:00 HST (not shown), consistent with the occurrence of maximum cloud water content. Weak sinking motions occur in the early morning (0200–04:00 HST), giving rise to a cloud water content minimum in the southwest lee (x ~ 38 km).

4.3. Kona Coast

[30] Onshore sea breezes/anabatic flow are observed to develop on the Kona coast during the daytime and offshore land breezes/katabatic flow at night [*Leopold*, 1949; *Chen and Nash*, 1994; *Yang and Chen*, 2003]. During the day (at night), a thermally direct secondary circulation cell is simulated in a similar model over the Kona area with the rising (sinking) motion over the slope and the sinking (rising) motion over the coastal region [*Yang et al.*, 2008b]. Figure 10a shows the time-height section of horizontal wind velocity just off the Kona coast. The westerly return flow in the wake is found in a quite deep layer reaching 800 hPa. Above this layer, the easterly trades prevail, enhanced (to 3 m s^{-1} at 750 hPa) by the upper return branch of the sea breeze circulation cell during the day and weakened (to 1 m s^{-1}) at night. As solar heating intensifies from morning to afternoon, clouds develop on the Kona slope with moisture upward transportation. The increased moisture over land is advected offshore by the easterly winds during the day in a deep layer from 850 to 600 hPa where humidity reaches the daily maximum at 14:00 HST, 1.5 g kg^{-1} higher than the nighttime minimum.

[31] The model simulates the offshore advection of increased moisture at 750 hPa from morning to afternoon, concurrent with the offshore propagation of clouds observed from satellite (Figure 4b). This offshore development of clouds off Kona coast during the afternoon is not simulated in the model (Figure 7c) but the offshore advection of moisture by the easterly trades leads us to suggest that the offshore KC cloud band is due to the advection of clouds that form on the Kona slope by the trades above 850 hPa. Different from the SW lee cloud band, there is probably little in situ cloud production for the KC cloud band as the offshore subsidence of the thermally direct circulation cell causes moisture to decrease between 950–850 hPa below the easterly wind layer during the day (Figure 10a). In the absence of local cloud production, cloud droplets evaporate quickly on their way offshore riding on the easterlies under high numerical mixing in the model. The rapid offshore decay of KC clouds is suggestive of strong dissipation in reality (Figure 4b), which includes subsidence and mixing. The offshore extent of the KC cloud band is much smaller than that of the SW lee cloud band, the latter featuring substantial in situ production in the convergence line.

[32] At night, katabatic flow and land breezes develop over the Kona area, advecting relatively dry air to the nearby waters off the coast and resulting in a diurnal minimum of mixing ratio at low levels below 950 hPa (Figure 10a). The convergence between the offshore/land breezes and the dynamically induced onshore flow causes rising motion in the wake. In the northern part of the cross-stream transect in Figure 11 (x ~ 10 km), the upward motion peaks around 2 am, leading to the nighttime increase in cloudiness off the Kona coast in the model (Figures 7f and 11b). Unlike the afternoon KC cloud band, the Kona cloud deck during night are surrounded by low ICW and likely supported by in situ production (Figures 7e and 7f). Indeed, the rising motion causes the nighttime increase in humidity between 950 and 850 hPa off the Kona coast (Figure 10a). We have diagnosed the source/sink term of cloud water content using the same method as for the afternoon SW lee cloud band, for a period from 0000 and 04:00 HST and a layer from the surface to 8 km. In the nighttime off-Kona

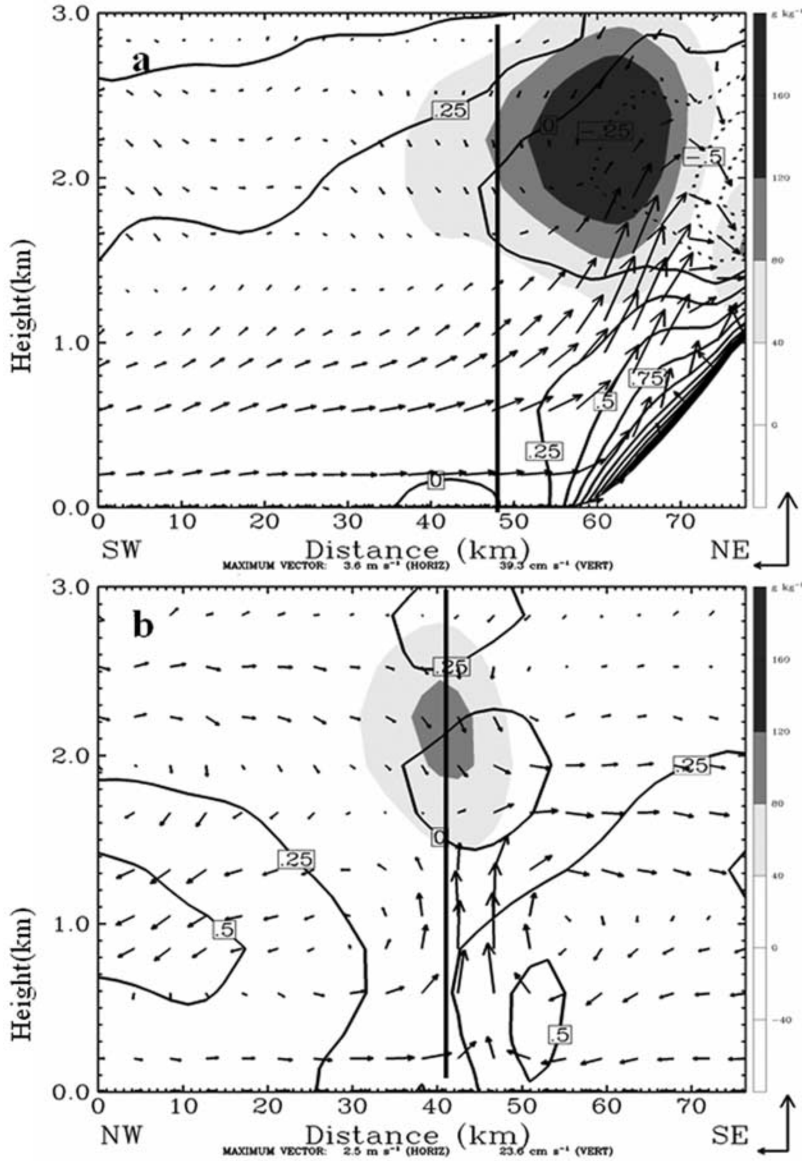

Figure 9. Along-stream cross-sections (the line CD in Figure 7f) for the difference in mean cloud water content (10^{-3} g kg^{-1}; shaded area), potential temperature (K, solid lines) with a contour interval of 0.25 K, and the mean wind vectors projected on the section plane and across-stream cross-sections (the line AB in Figure 7c) between 14:00 HST and 02:00 HST in the summer of 2005. Maximum horizontal and vertical wind speeds are 3.6 and 0.4 m s^{-1}, respectively. The thick straight solid line in Figure 9a shows the position of the cross-section in Figure 9b, while Figure 9b shows the position of the cross-section in Figure 9a. Note that the lower panels cover part of the wind wake (distance <30 km).

cloud deck, local production is 2–3 times greater than horizontal advection (not shown).

5. Sensitivity to Trade Wind Strength

[33] This section investigates how cloud patterns change in response to variability in trade wind strength, thereby gaining further insights into cloud formation mechanisms. We classify strong and weak trade wind days in summers of 2004 and 2005 using wind velocity at 1000 and 925 hPa at 4 grid points about 200–300 km upstream of Hawaii from the GFS 1° × 1° analysis at 14:00 HST. A strong (weak) trade wind day is when the wind speed is larger (smaller) than 8.5 m s^{-1} (6.5 m s^{-1}) with a direction between 70° and 90° from the north. With these criteria, 16 and 15 strong trade wind days are chosen in 2005 and 2004, respectively while there are 16 and 14 weak trade wind days in 2005 and 2004, respectively. We use these classifications for the analysis of model output during the summer of 2005. The criteria result in 5 strong and 5 weak trade wind days in August 2005 for the GOES-10 analysis.

5.1. Satellite Observations

[34] The trade wind inversion height is an important factor for cloud cover over and near Hawaii (not shown). For MODIS cloud composites, we impose an additional

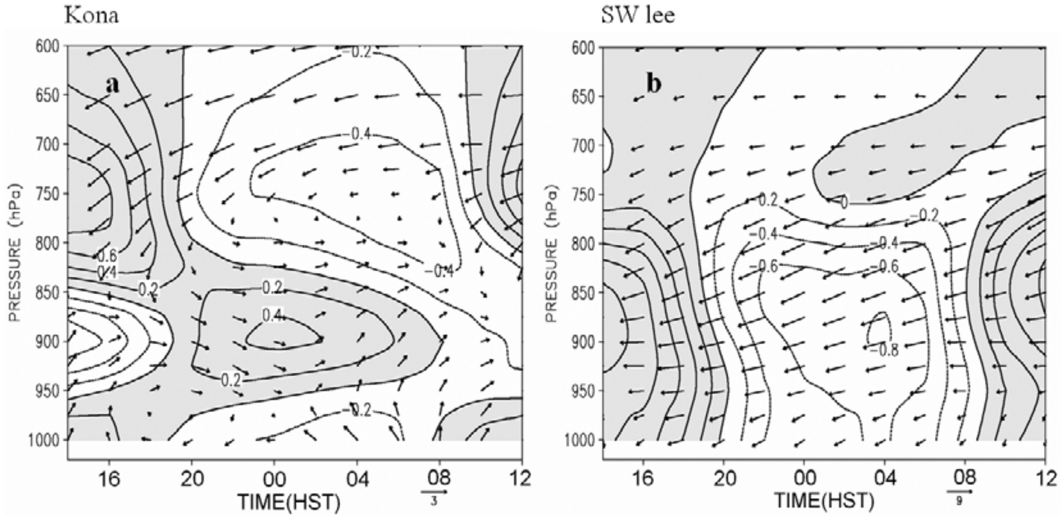

Figure 10. Time-Height sections of the total horizontal wind velocity (vectors in m s^{-1}) and water vapor mixing ratio (g kg^{-1}; shade > 0) deviations from the daily mean at (a) 156°W, 19.5°N (S1 in Figure 7c) off of Kona and (b) 155.95°W, 19°N (S2 in Figure 7f) off of the southwest coast.

requirement that the inversion height falls between 1600 and 2550 m in the soundings of Lihue, Kauai to minimize the effect of inversion height variability. These criteria give only 10 in 2005 and 9 in 2004 strong trade wind days, and 9 in 2005 and 9 in 2004 weak trade wind days. The low-level winds upstream of Hawaii are about 4 m s^{-1} larger for the strong than weak trade wind days while maintaining a nearly easterly direction in both composites (Figure 12).

[35] In the afternoon, the KC cloud band extends farther offshore in the strong than weak trade wind composites (Figure 13) as the easterly winds increase by 0.5–1 ms^{-1} at 750 hPa in the model (not shown). The SW lee cloud band also extends farther southwestward under stronger trades, a change more clearly seen in GOES cloud albedo (Figures 14a and 14b). The broad cloud band further downstream in the wake (west of 157°W), however, is more organized in the weak than strong trade wind composite (Figure 13).

[36] Afternoon cloudiness on the windward side increases and expands greatly in the offshore direction under strong trade winds (Figures 13 and 14), consistent with increased upward motion there in the model (Figure 15b). Over the island, increased orographic up/downdrafts sharpen variations in cloudiness across major mountain ridges in response to increased winds. Lee of Kohala Mountains in the northwest Hawaii and the Kilauea Volcanoes in the southeast, and on the leeside slope of Humu'ula Saddle between Mts. Kea and Loa, cloud frequency is lower for strong than weak trade wind days (Figures 13 and 14).

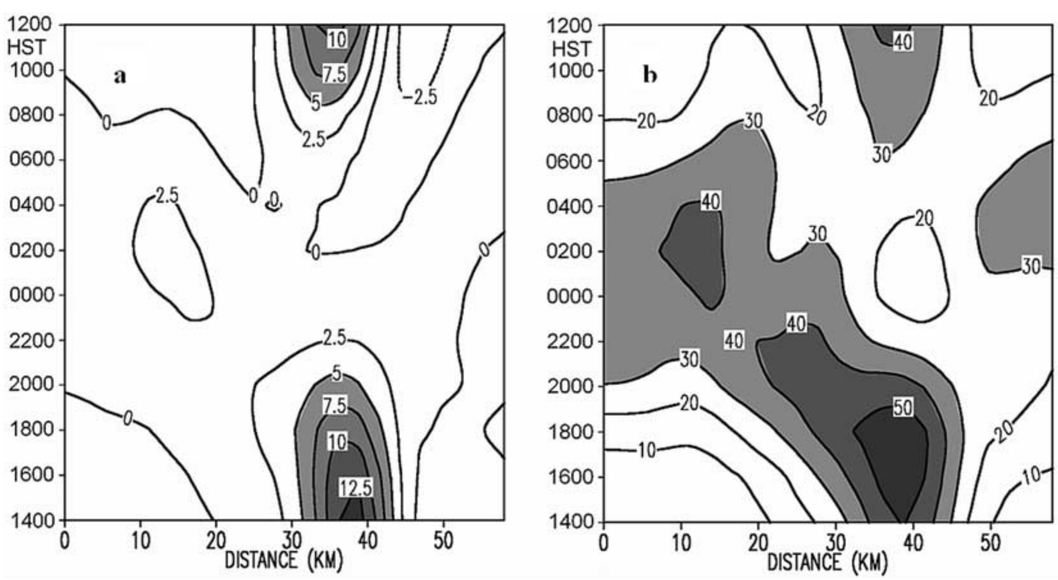

Figure 11. Diurnal cycle of (a) vertical velocity (cm s^{-1}) at 500 m and (b) cloud water content (g kg^{-1}) at 2200 m above the sea level across the trade wind flow (the line in Figure 7c). The distance is from northwest to southeast. Note that the left part of the figures is in the wind wake (distance <30 km).

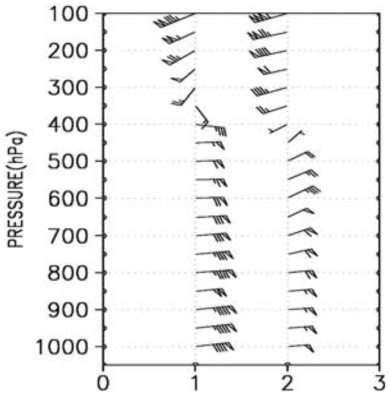

Figure 12. Wind profiles from GFS 1° × 1° analysis at 4 grid points 200–300 km upstream of Hawaii for (left) strong and (right) weak trade wind days during the summers of 2004 and 2005. Pennants, full barbs, and half barbs represent 5, 1, and 0.5 m s^{-1}, respectively.

[37] At night, temperature maxima (or cloudiness minima) are found over the northwestern and southwestern leeward waters for both strong and weak trade wind days. IR temperature in these leeside areas is 1–2 K higher for the strong than weak trade wind days, because of stronger adiabatic descent of the trade wind flow aloft. In the SW lee, in particular, clear sky conditions prevail at nights of strong trades with a well-defined band of high IR temperature, in great contrast to a long cloud band emanating from Kauna Point in the afternoon (Figures 14a and 14c).

[38] Off the Kona coast, IR temperature is lower by 1 K (with more clouds) during night for the strong than weak trade wind days (Figures 14c and 14d), supporting the hypothesis of *Yang and Chen* [2003] that more rainfall/cloud production occurs along the Kona coast at night as a result of enhanced convergence between the stronger dynamically induced westerly return flow in the wake and the offshore/land breezes. In the strong wind composite, a well-defined band of low IR temperature, sandwiched by high IR temperatures to the north and south, extends from the Kona coast westward. This cloud band off the Kona coast may connect with the broad cloud band further to the west (Figure 13), forming a long continuous cloud band from the island along the center axis of the wake as discussed by *Smith and Grubišić* [1993]. Such a continuous cloud band probably exists only during night to early morning as the subsidence prevails the wake near the Kona coast during the day.

5.2. Numerical Simulation

[39] Figure 15 shows the differences in the horizontal winds at 500 m and vertical velocity at 750 m above the sea level between strong and weak trades. For the daily mean (Figure 15a), the large wind speed differences are found to the north and south of the island with the maximum up to 7 m s^{-1}, as opposed to a 4 m s^{-1} difference in the upstream wind speed (Figure 12). In the wake off the Kona coast, the westerly reverse flow is 1–3 m s^{-1} stronger for the strong than weak trade wind days. The rising motions in the northwestern and southwestern leeward areas are stronger for the strong trade wind days. The rising motion maximum in the northwest lee is related to the hydraulic jump of the trade wind flow. When the trades are stronger, so is the hydraulic jump [*Yang et al.*, 2008b]. Over the southwestern lee, the rising motions near the coast are related to the hydraulic jump, and then extend far downstream in the convergence zone where the trade wind flow and the northerly component of the winds in the southern wake meet. The daily mean composite difference between strong and weak trades indicates that the SW lee convergence is partly due to the dynamical forcing of island orography.

[40] The patterns at 14:00 HST are generally similar to the daily mean (Figure 15) but the upward velocity is significantly stronger in the afternoon in the SW lee convergence line (Figure 15b). In the wake, the northwesterly winds intensify in the afternoon blowing toward the convergence line for the strong trades. As a result, the vertical velocity at 14:00 HST is 5–10 cm s^{-1} stronger than the daily mean. Thus the effects of trade wind strength on the lee circulations are modified by land surface heating during the day, which can affect the boundary layer stratification or the Froude number, for example. The intensification of rising motions in the southwestern lee is consistent with increased cloudiness there in the afternoon for the strong trade wind days.

6. Summary

[41] We have used polar-orbiting (MODIS) and geostationary (GOES-10) satellites to map the summer cloud

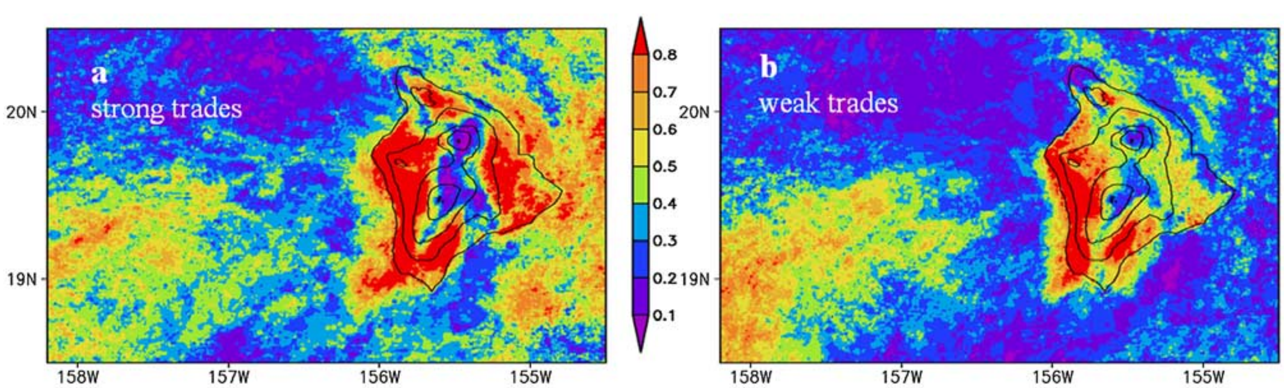

Figure 13. Cloud frequency from MODIS Terra at 14:00–15:00 HST for (a) 19 strong and (b) 18 weak trade wind days during the summers of 2004 and 2005.

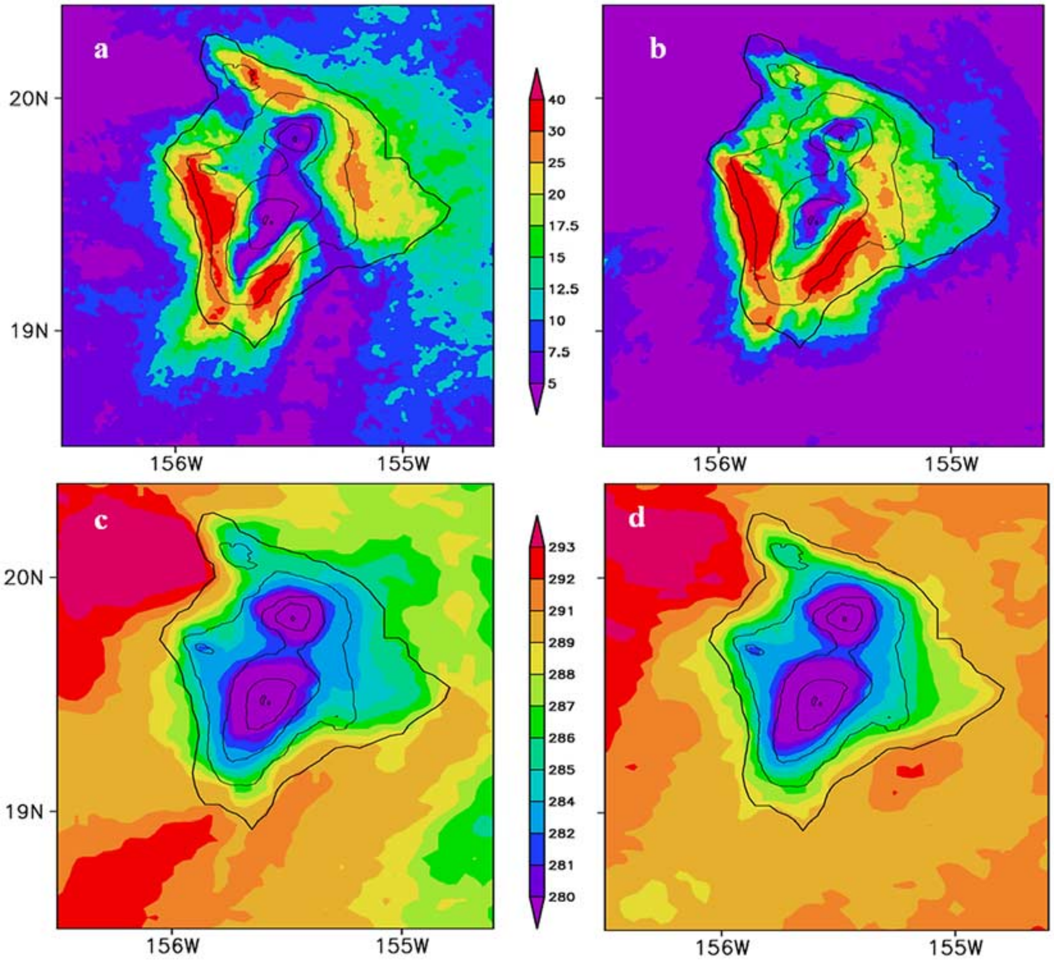

Figure 14. Effective albedo (%) at 14:00 HST during August 2005 from GOES-10 visible channel for (a) 6 strong and (b) 6 weak trade wind days. Mean temperature (K) at 02:00 HST during August 2005 from GOES-10 IR channel-5 for (c) 6 strong and (d) 6 weak trade wind days.

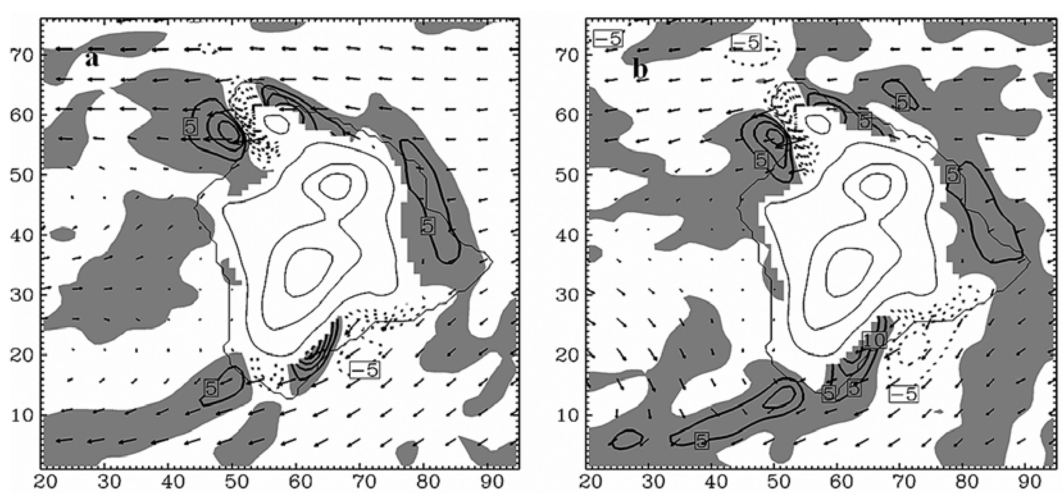

Figure 15. Horizontal (vectors) and vertical velocity (contours in cm s^{-1}; shade > 0) difference at 500 m above the sea level between 16 strong and 16 weak trade wind days: (a) daily mean and (b) at 14:00 HST. The maximum vector is 9 m s^{-1}.

climatology, and MM5/LSM simulation to investigate the cloud formation mechanisms lee of Hawaii Island. Our results show that both the dynamical and thermal forcing of the island is important. With mountaintops much higher than the trade wind inversion, the island splits the northeast trades and forces a "flow-around" regime characterized by a westerly reverse flow in the wake. Orographic effects are clearly manifested in the cloud climatology over land: orographic lifting keeps cloud occurrence high on the windward slopes and the southeast slope of Mt. Loa while persistent descents prevent cloud from forming lee of the ridges of Kohala Mountains, the Kilauea volcanoes, and the Mt. Loa's south extension. Standing above the inversion, cloud occurrence is low on both Mts. Loa and Kea.

[42] During the day, clouds develop over land on the Kona slope from the morning to afternoon as part of the sea breeze/anabatic flow system. The wake within 100 km off the Kona coast is nearly free of clouds during the day except on and immediately (~20 km) off the coast where a Kona cloud band develops in the afternoon as the easterly trades blow cloud droplets offshore from land in a layer above the westerly reverse flow. The model fails to simulate this KC cloud band because of too strong dissipation but captures the daytime humidity increase in the cloud layer. At night, a cloud deck develops on and off the Kona coast as the offshore land breezes converge onto the westerly reverse flow in the wake. This nighttime cloud deck brings rainfall on the Kona coast, which is confirmed by land station observations.

[43] In the southwest lee of the island, our combined analysis of observations and model simulation reveals a southwest-tilted line of convergence and clouds during the daytime, a new finding not discussed in the literature. Satellite observations show that the SW lee cloud band, extending a few tens of km offshore from Kauna Point, is most pronounced in the afternoon and vanishes during night. The model results indicate that the in situ cloud production is important as the ascending motion transports moisture upward in the convergence line. The SW lee convergence intensifies as sea breezes/anabatic flow meets there from three directions: from the west and southeast slopes of Mt. Loa, and perpendicular to the coast from the southwest. Besides this diurnal cycle, wind convergence shows a more pronounced downstream extension in the southwest than northwest lee even in the daily mean, a north-south asymmetry that we suggest is due to the Coriolis effect on the orographic flow. Acting on the orographic acceleration/deceleration of the easterly flow, the Coriolis force induces a cross-stream component that leads to convergence on the southern and divergence on the northern edge of the wake [e.g., *Hunt et al.*, 2001]. Further investigations are necessary into the dynamics of the SW lee convergence and its diurnal cycle.

[44] Mountain height relative to the trade wind inversion determines the lee circulation regime, which in turn shapes the cloud pattern in the wake. The flow regime dependency of cloud formation is illustrated by comparison with the study of *Yang et al.* [2008a], a companion paper on cloud patterns lee of smaller and shorter Hawaiian islands of Kauai and Oahu. Standing below the inversion, these islands generate a flow-over regime with the reduced easterly flow in the wake. In the wakes of Kauai and Oahu

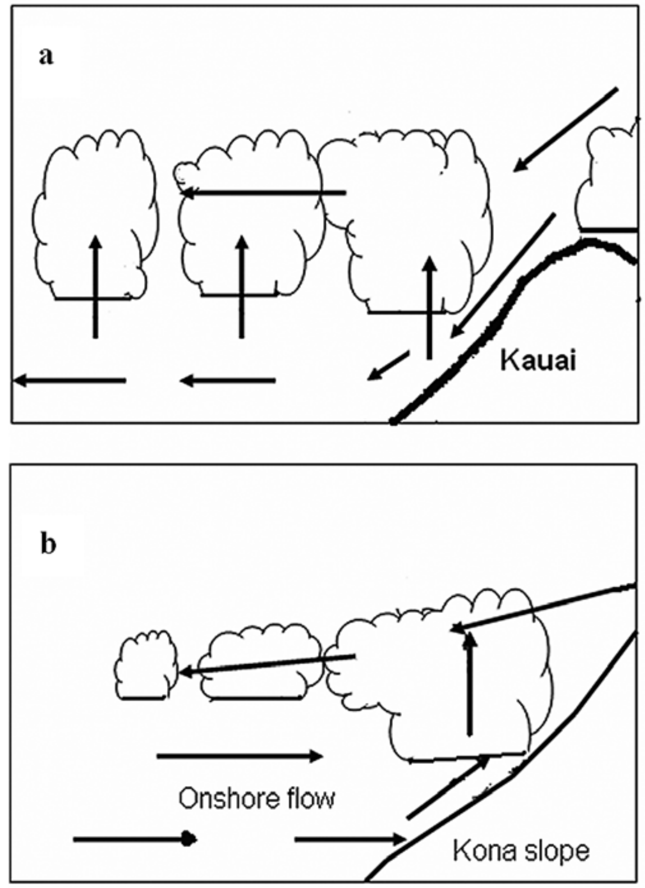

Figure 16. Schematics of afternoon cloud formation in the wakes of (a) short Kauai and (b) tall Hawaii Islands.

during afternoon, the easterlies advect warm air from the islands, lowering the surface pressure and inducing a surface convergence that anchors a long trail of clouds (Figure 16a). In the wake of tall Hawaii Island, the westerly onshore flow prevents thermal advection from the island, resulting in a cool wake during afternoon compared to the northwest and southwest lees where warm air is advected from the island by the strong trades. In the cool wake, divergence prevails and cloudiness is low during the day except some afternoon clouds advected from the Kona coast by the easterlies around the inversion base (Figure 16b).

[45] Both dynamical and thermal forcing of the Hawaiian Islands is important for lee cloud formation, the latter effect manifested in the pronounced diurnal cycle in cloud distribution. The cloud pattern difference between Kauai/Oahu and Hawaii Islands are equally striking at night. The cold advection from the islands cools the wakes of Kauai and Oahu, and the resultant high pressure and divergence suppress clouds. In the Hawaii wake, by contrast, the convergence between the westerly reverse flow and offshore land breezes leads to the formation of a nighttime cloud deck.

[46] **Acknowledgments.** This study is supported by the NOAA PRIDE Program, NASA, and JAMSTEC. The authors wish to thank the NCAR MM5 group for the applications of the MM5/LSM, Dr. P. Hacker for encouragement and Dr. Y.-L. Chen for useful discussion at the early stage of this study. IPRC publication 523 and SOEST publication 7460.

References

Carbone, R. E., J. D. Tuttle, W. A. Cooper, V. Grubiši, and W. C. Lee (1998), Trade wind rainfall near the windward coast of Hawaii, *Mon. Weather Rev.*, *126*, 2847–2863.

Chen, F., and J. Dudhia (2001), Coupling an advanced land surface-hydrology model with the Penn State-NCAR MM5 modeling system. part I: Model implementation and sensitivity, *Mon. Weather Rev.*, *129*, 569–585.

Chen, Y.-L., and A. J. Nash (1994), Diurnal variations of surface airflow and rainfall frequencies on the island of Hawaii, *Mon. Weather Rev.*, *122*, 34–56.

Chelton, D. B., M. G. Schlax, M. H. Freilich, and R. F. Milliff (2004), Satellite measurements reveal persistent small-scale features in ocean winds, *Science*, *303*, 978–983.

Dudhia, J. (1993), A nonhydrostatic version of the Penn state-NCAR mesoscale model: Validation tests and simulation of an Atlantic cyclone and cold front, *Mon. Weather Rev.*, *121*, 1493–1513.

Dudhia, J., and M. W. Moncrieff (1989), A three-dimensional numerical study of an Oklahoma squall line containing right-flank supercells, *J. Atmos. Sci.*, *46*, 3363–3391.

Foote, D. E., E. L. Hill, S. Nakamura, and F. Stephens (1972), *Soil Survey of Islands of Kauai, Oahu, Maui, Molokai, and Lanai, State of Hawaii*, 115 pp., Soil Conservation Service, U.S. Dept. of Agriculture, in cooperation with the University of Hawaii Agricultural Experiment Station, Natural Resources Conservation Service, U.S. Dept. of Agriculture, Honolulu, HI.

Hafner, J., and S.-P. Xie (2003), Far-field simulation of the Hawaiian wake: Sea surface temperature and orographic effects, *J. Atmos. Sci.*, *60*, 3021–3032.

Hong, S.-Y., and H. L. Pan (1996), Nonlocal boundary layer vertical diffusion in a medium-range forecast model, *Mon. Weather Rev.*, *124*, 2322–2339.

Hsie, E.-Y., R. A. Anthes, and D. Keyser (1984), Numerical simulation of frontogenesis in a moist atmosphere, *J. Atmos. Sci.*, *41*, 2581–2594.

Hunt, J. C. R., H. Olafsson, and P. Bougeault (2001), Coriolis effects on orographic and mesoscale flows, *Q. J. R. Meteorol. Soc.*, *127*, 601–633.

Leopold, L. B. (1949), The interaction of trade wind and sea breeze, Hawaii, *J. Meteorol.*, *8*, 533–541.

Nickerson, E. C., and M. A. Dias (1981), On the existence of atmospheric vortices downwind of Hawaii during the HAMEC project, *J. Appl. Meteorol.*, *20*, 868–873.

Olafsson, H., and P. Bougeault (1997), The effects of rotation and surface friction on orographic drag, *J. Atmos. Sci.*, *54*, 193–210.

Patzert, W. C. (1969), Eddies in Hawaiian waters, *HIG Rep. No. HIG-69-8*, 51 pp., Hawaii Institute of Geophysics, University of Hawaii, Honolulu.

Reinecke, P. A., and D. R. Durran (2008), Topographic blocking in flows with non-uniform upstream static-stability profiles, *J. Atmos. Sci.*, *65*, 1035–1048.

Sakamoto, T. T., A. Sumi, S. Emori, T. Nishimura, H. Hasumi, T. Suzuki, and M. Kimoto (2004), Far-reaching effects of the Hawaiian Islands in the CCSR/NIES/FRCGC high-resolution climate model, *Geophys. Res. Lett.*, *31*, L17212, doi:10.1029/2004GL020907.

Sasaki, H., and M. Nonaka (2006), Far-reaching Hawaiian lee countercurrent driven by wind-stress curl induced by warm SST band along the current, *Geophys. Res. Lett.*, *33*, L13602, doi:10.1029/2006GL026540.

Sato, H. H., W. Ikeda, R. Paeth, R. Smythe, and M. Takehiro Jr. (1973), *Soil Survey of the Island of Hawaii, State of Hawaii*, 232 pp., Soil Conservation Service, U.S. Dept. of Agriculture, in cooperation with the University of Hawaii Agricultural Experiment Station, Natural Resources Conservation Service, U.S. Dept. of Agriculture, Honolulu, HI.

Schroeder, T. (1993), Climate controls, in *Prevailing Trade Winds*, edited by M. Sanderson, pp. 12–36, University of Hawaii Press, Honolulu, Hawaii.

Shen, B.-W., R. Atlas, J.-D. Chern, O. Reale, S.-J. Lin, T. Lee, and J. Chang (2006), The 0.125 degree finite-volume general circulation model on the NASA Columbia supercomputer: Preliminary simulations of mesoscale vortices, *Geophys. Res. Lett.*, *33*, L05801, doi:10.1029/2005GL024594.

Smith, R. B. (1989), Hydrostatic airflow over mountains, in *Advances in Geophysics*, vol. 31, pp. 1–41, Academic Press, New York.

Smith, R. B., and V. Grubišić (1993), Aerial observation of Hawaii's wake, *J. Atmos. Sci.*, *50*, 3728–3750.

Smolarkiewicz, P. K., and R. Rotunno (1989), Low Froude number flow past three-dimensional obstacles. part I: Baroclinically generated lee vortices, *J. Atmos. Sci.*, *46*, 1154–1164.

USGS (1986), Land use land cover digital data from 1:250, 000 and 1:100, 000-scale maps, in *Data User Guide 4*, 35 pp., U.S. Geological Survey, Reston, VA.

Xie, S.-P., W. T. Liu, Q. Liu, and M. Nonaka (2001), Far-reaching effects of the Hawaiian Islands on the Pacific Ocean-atmosphere, *Science*, *292*, 2057–2060.

Yang, Y., and Y.-L. Chen (2003), Circulations and rainfall on the leeside of the island of Hawaii during HaRP, *Mon. Weather Rev.*, *131*, 2525–2542.

Yang, Y., and Y.-L. Chen (2008), Effects of terrain heights and sizes on island-scale circulations and rainfall for the island of Hawaii, *Mon. Weather Rev.*, *136*, 120–146.

Yang, Y., Y.-L. Chen, and F. M. Fujioka (2005), Numerical simulations of the island induced circulations for the island of Hawaii during HaRP, *Mon. Weather Rev.*, *133*, 3693–3713.

Yang, Y., S.-P. Xie, and J. Hafner (2008a), The thermal wake of Kauai Island: Satellite observations and numerical simulations, *J. Clim.*, in press.

Yang, Y., Y.-L. Chen, and F. M. Fujioka (2008b), Effects of trade-wind strength and directions on the leeside circulations of the island of Hawaii, *Mon. Weather Rev.*, with minor revision.

Yu, Z., N. Maximenko, S.-P. Xie, and M. Nonaka (2003), On the termination of the Hawaiian lee countercurrent, *Geophys. Res. Lett.*, *30*(5), 1215, doi:10.1029/2002GL016710.

Zhang, Y., Y.-L. Chen, S.-Y. Hong, K. Kodama, and H.-M. H. Juang (2005), Validation of the coupled NCEP mesoscale spectral model and an advanced land surface model over the Hawaiian Islands. part I: Summer trade wind conditions over Oahu and a heavy rainfall events, *Wea. Forecasting*, *20*, 827–846.

J. Hafner and S.-P. Xie, International Pacific Research Center, SOEST, University of Hawaii at Manoa, 1680 East West Road, POST Bldg. #401 Honolulu, HI 96822, USA.

Y. Yang, National Institute of Water and Atmosphere Research, 301 Evans Bay Parade, Hataitai, Wellington, New Zealand. (yang.yang816@gmail.com)